Space Weather

RESEARCH ARTICLE
10.1029/2021SW002764

Special Section:
Space Weather Impacts on Electrically Grounded Systems at Earth's Surface

The Impact of Sudden Commencements on Ground Magnetic Field Variability: Immediate and Delayed Consequences

Andrew W. Smith[1], Colin Forsyth[1], Jonathan Rae[2], Craig J. Rodger[3], and Mervyn P. Freeman[4]

[1]Mullard Space Science Laboratory, UCL, Dorking, Surrey, UK, [2]Department of Mathematics, Physics and Electrical Engineering, Northumbria University, Newcastle upon Tyne, UK, [3]Department of Physics, University of Otago, Dunedin, New Zealand, [4]British Antarctic Survey, Cambridge, UK

Key Points:

- Sudden Commencements (SCs) are linked to 25% of rates of change above 50 nT min^{-1} at low geomagnetic latitudes, for example, <10°
- 90% of fluctuations above 50 nT min^{-1} occur within 3 days of an SC below 60° latitude
- Only Storm Sudden Commencements have a link with elevated rates of change of the field, either during the SSC or in the following days

Correspondence to:
A. W. Smith,
andy.w.smith@ucl.ac.uk

Citation:
Smith, A. W., Forsyth, C., Rae, J., Rodger, C. J., & Freeman, M. P. (2021). The impact of sudden commencements on ground magnetic field variability: Immediate and delayed consequences. *Space Weather*, *19*, e2021SW002764. https://doi.org/10.1029/2021SW002764

Received 16 MAR 2021
Accepted 8 JUN 2021

Abstract We examine how Sudden Commencements (SCs) and Storm Sudden Commencements (SSCs) influence the occurrence of high rates of change of the magnetic field (R) as a function of geomagnetic latitude. These rapid, high amplitude variations in the ground-level geomagnetic field pose a significant risk to ground infrastructure, such as power networks, as the drivers of geomagnetically induced currents. We find that rates of change of ~30 nT min^{-1} at near-equatorial stations are up to 700 times more likely in an SC than in any random interval. This factor decreases with geomagnetic latitude such that rates of change around 30 nT min^{-1} are only up to 10 times more likely by 65°. At equatorial latitudes we find that 25% of all R in excess of 50 nT min^{-1} occurs during SCs. This percentage also decreases with geomagnetic latitude, reaching ≤1% by 55°. However, the time period from the SC to 3 days afterward accounts for ≥90% of geomagnetic field fluctuations over 50 nT min^{-1}, up to ~60° latitude. Above 60°, other phenomena such as isolated substorms account for the majority of large R. Furthermore, the elevated rates of change observed during and after SCs are solely due to those classified as SSCs. These results show that SSCs are the predominant risk events for large R at mid and low latitudes, but that the risk from the SC itself decreases with latitude.

Plain Language Summary Rapid changes in the Earth's magnetic field can create the conditions for anomalous and potentially dangerous currents in spatially large networks such as power lines and pipelines. One phenomenon that can cause such rapid changes in the magnetic field are Sudden Commencements (SCs), driven by interplanetary shocks impacting the Earth's magnetosphere. In this work, we assess the risk due of SCs, finding that they contribute a significant fraction of large rates of change of the ground field at mid and low latitudes. SCs may also be followed by geomagnetic storms, and if we consider both the short SC intervals as well as a 3-day period that follows we can account for the vast majority of large rates of change of the geomagnetic field, at mid and low latitudes. This work should help guide hazard estimates for energy providers, for example the time period after an SC in which they could expect large and potentially dangerous currents.

1. Introduction

One of the main pathways through which Space Weather can impact society is through damage to ground-based infrastructure caused by the generation of Geomagnetically Induced Currents (GICs). GICs originate from the induced Ground Electric Field (GEF), which itself is driven by high amplitude magnetic field fluctuations and geological conductivity gradients. GICs can be generated in any long grounded conductor, including power grids, pipelines or rail networks (Boteler et al., 1998). Modern society is fundamentally dependent upon the reliable delivery of power, and Space Weather is therefore a critical risk factor for such operations (e.g., Committee on the Peaceful Uses of Outer Space (COPUOS), 2017; Eastwood et al., 2018). The impact of widespread power network failure has been estimated at billions of US dollars a day (Oughton et al., 2017, 2019).

Direct measurements of GICs in infrastructure are sparse, either due to their commercial sensitivity or expense in performing the observations. The South Island of New Zealand is a notable exception (e.g., Mac Manus et al., 2017; Marshall et al., 2012; Rodger et al., 2017). Indirect observations of GICs in power lines

are also possible, using techniques such as the differential magnetometer method (e.g., Campbell, 1980; Hübert et al., 2020; Viljanen & Pirjola, 1994); however, these measurements are also sparse since additional equipment needs to be deployed and data analyzed. Therefore, for geographically widespread and longtime interval studies a substitute measurement is required.

The magnitude of GICs in a given power network is dependent upon three main factors: the rate of change of the surface magnetic field, the orientation and properties of the power network and the local geology (i.e., the subsurface conductivity) (Bedrosian & Love, 2015; Beggan, 2015; Divett et al., 2018; Thomson et al., 2005; Viljanen et al., 1999, 2013, 2013). The time scales of magnetic field variability have also been shown to be significant, with certain frequencies of magnetic field variability showing the best match with observed GICs (Clilverd et al., 2020; Oyedokun et al., 2020). However, in general, larger rates of change of the geomagnetic field will drive larger GICs (Viljanen et al., 2001). Indeed recent concurrent measurements from New Zealand have confirmed that the rate of change of the horizontal magnetic field is very well correlated with the observed GIC magnitude (Mac Manus et al., 2017; Rodger et al., 2017). Since the ground-level magnetic field has been consistently measured around the globe for many decades, this provides an appropriate proxy data set to statistically examine the potential likelihood of large GICs at different latitudes.

There are a plethora of phenomena, ultimately driven by the interaction between the solar wind and the Earth's magnetosphere, that can result in elevated rates of change of the ground magnetic field. On the largest spatial and temporal scales, geomagnetic storms are driven by significant periods of enhanced coupling between the solar wind and magnetosphere, typically by Coronal Mass Ejections (CME) and their surrounding medium (Borovsky & Denton, 2006; Kilpua et al., 2019; Richardson & Cane, 2012). For many years geomagnetic storms and related smaller-scale storm associated dynamical processes have been linked to variations in the geomagnetic field, and further to induced currents (Dimmock et al., 2019; Kappenman, 1996; Kappenman & Albertson, 1990; Ngwira, Pulkkinen, Leila Mays, et al., 2013; Pulkkinen et al., 2005). On a shorter time scale of hours, geomagnetic substorms, which manifest as cycles of energy storage and release in the magnetosphere (e.g., Akasofu, 1964; McPherron et al., 1973; Tanskanen et al., 2002), are also associated with the generation of dynamic ionospheric currents. Substorms are sporadic and intermittent, but tend to recur on time scales of ∼2–4 h during periods of strong solar wind driving (Forsyth et al., 2015; Freeman & Morley, 2004; Huang et al., 2004; Lee et al., 2006; Morley et al., 2009). While ionospheric currents vary with local season, the average additional dynamic currents resulting from substorms are similar throughout the year (Forsyth et al., 2018). The strong and dynamic ionospheric substorm currents often correspond to large changes in the geomagnetic field (Engebretson et al., 2021; Freeman et al., 2019; Turnbull et al., 2009; Viljanen et al., 2001), and GICs (Viljanen et al., 2006). Studies have shown that high-latitude surface magnetic field perturbations, and the field-aligned currents that drive them, react to the solar wind on different characteristic time scales: ranging between 10 and 150 min depending on location (e.g., Coxon et al., 2019; Shore et al., 2019).

In contrast to the energy storage and release processes within a substorm, some intervals of large ground magnetic variability can be driven by much more immediate changes in the impinging solar wind, for example, Sudden Commencements (SCs). SCs are rapid increases in the northward component of the ground magnetic field (Araki, 1977; Araki et al., 1997; Chree, 1925), signaling the response of the magnetosphere to the impact of a solar wind pressure pulse or shock (Fiori et al., 2014; Lühr et al., 2009; Oliveira & Samsonov, 2018; Takeuchi et al., 2002). Such changes in the geomagnetic field have also been commonly noted to generate large GICs (e.g., Beland & Small, 2004; Carter et al., 2015; Kappenman, 2003; Marshall et al., 2012; Oliveira et al., 2018; Rodger et al., 2017; Zhang et al., 2015). These interplanetary shocks may be driven by structures such as CMEs, and so while the initial shock may drive or instigate immediate magnetospheric activity, it may also herald the start of a longer interval of enhanced coupling between the solar wind and magnetosphere—the geomagnetic storm, that includes a wide range of magnetospheric phenomena such as geomagnetic substorms (Akasofu & Chao, 1980; Gonzalez et al., 1994; Kokubun et al., 1977; Yue et al., 2010; Zhou & Tsurutani, 2001). An SC that is followed by a geomagnetic storm is referred to as a Storm Sudden Commencement (SSC).

Rogers et al. (2020) recently used extreme value theory to show that the distribution of return rates of extreme surface magnetic field variability vary significantly with local time and latitude, with evidence

for distinct driving phenomena being discernible. For example, at low latitudes a class of extreme rates of change of the field were mostly northward directed, and therefore likely attributable to SCs. Meanwhile, several authors have shown that the magnitude of extreme geomagnetic fluctuations (at the 100–200 years return level) maximize between ∼50° and 60° geomagnetic latitude, corresponding to the maximum equatorward extent of the auroral electrojets (Ngwira, Pulkkinen, Wilder, et al., 2013; Rogers et al., 2020; Thomson et al., 2011). While these large scale patterns are observed, it should be noted that local effects, either from sharp spatial conductivity changes or small-scale ionospheric currents, may also have a significant effect on the precise measured magnetic field variability (e.g., Dimmock et al., 2020; Ngwira et al., 2015). It is therefore of crucial importance to consider the variability of the magnetic field as a function of both local time and latitude.

Recently, Freeman et al. (2019) and Smith et al. (2019) assessed the relative contribution of substorms and SCs (respectively) to extreme ground magnetic field variability at the mid-latitude UK magnetometer stations. Freeman et al. (2019) found that 54%−56% of extreme (≥99.97th percentile) ground fluctuations in the UK were associated with substorm expansion and recovery phases, explaining a large portion of such variability, but leaving a relatively large fraction unattributed. Meanwhile, Smith et al (2019) showed that only a small fraction (≤8%) of extreme rates of change of the geomagnetic field were associated directly with SCs, but that 90% of all extreme fluctuations were observed in the 3 days following SSCs, thereby including each SSC's storm and component substorms that are causally related to the same solar wind structures. The scope of the study by Smith et al. (2019) was extremely limited in latitude, only considering three mid-latitude, UK based stations. In this work, we expand this scope to consider the relative impact of SCs on ground magnetic field variability at a large number of magnetometer stations. In particular, we assess how the impact of SCs varies with geomagnetic latitude. The study is structured as follows. First, in Section 2 we outline the data and definitions used by the study. In Section 3 we discuss the results of the study, while in Section 4 we discuss our results in terms of the latitudinal dependence observed, the type of magnetospheric response and consequences for forecasting GICs. Section 5 then summarizes the study.

2. Data

In this study, we utilize 1 min resolution data from a collection of INTERMAGNET observatories. We have selected magnetometer stations as close in longitude to the three UK based stations in the original study of Smith et al. (2019) as possible, while attempting to maximize our latitudinal coverage. In this way we attempt to minimize any local time effects that could be present (Rogers et al., 2020). We further require that data from the observatory is available for the full interval between 1996 and 2016 (inclusive), which forms the basis of our statistical study. As SCs are a stochastic phenomenon, it is vital to ensure the data set and events are identical between stations. A map of the 12 stations fulfilling these criteria is shown in Figure 1, Table 1 provides further details. The geomagnetic latitudes were calculated using the International Geomagnetic Reference Field (IGRF) 2010 model. While we have attempted to cover as broad a latitudinal range as possible, it can be seen that the region between 44° and 65° geomagnetic latitude is fairly densely represented, while there is a gap between 7° and 44°. Nonetheless, this selection of stations provides us with adequate latitudinal sampling (as will be shown) and the long interval of data necessary for this study.

2.1. Rate of Change

We define the horizontal geomagnetic field as $\mathbf{H} = (X, Y)$, where X and Y are the northward and eastwards components respectively. We then define the one-minute rate of change of the horizontal geomagnetic field (R) as:

$$R = \frac{\delta \mathbf{H}}{\delta t} = \frac{\sqrt{\left[X(t+\delta t) - X(t)\right]^2 + \left[Y(t+\delta t) - Y(t)\right]^2}}{\delta t} \quad (1)$$

in order to capture directional changes as well as changes in magnitude, following the definition used by several studies in the literature (e.g., Freeman et al., 2019; Smith et al., 2019; Viljanen et al., 2001). This

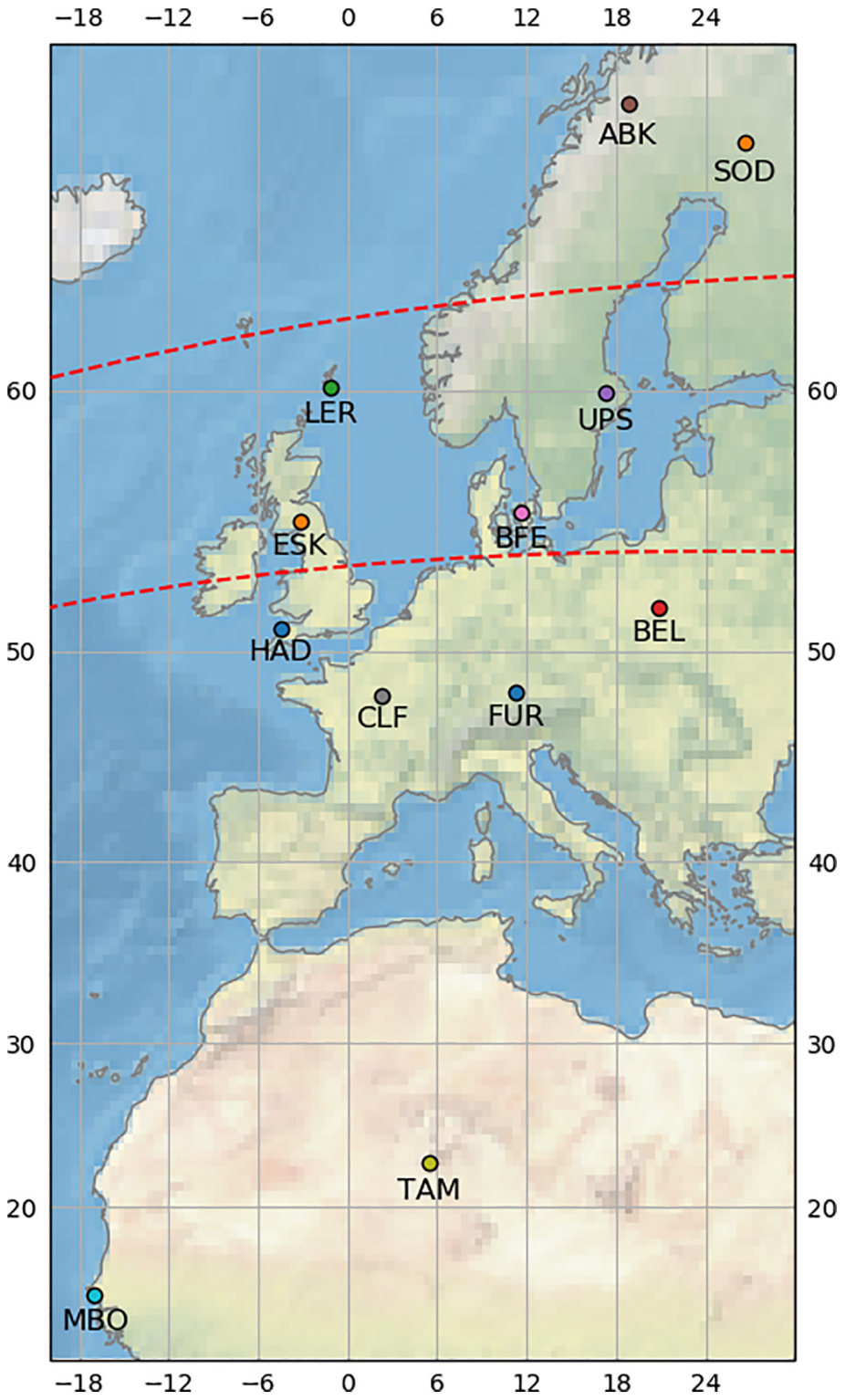

Figure 1. A geographical map of the 12 INTERMAGNET observatories included in this statistical study. The geomagnetic latitudes of 50° and 60° north are indicated with dashed red lines for reference. These geomagnetic latitudes have been calculated using a quasi-dipole model.

Table 1
INTERMAGNET Observatories Included in This Study

Station code	Station name	Geomagnetic latitude	Geomagnetic longitude
ABK	Abisko	65.18	101.82
SOD	Sodankyla	63.81	107.29
LER	Lerwick	57.85	81.15
UPS[a]	Uppsala[a]	56.34	95.90
ESK	Eskdalemuir	52.86	77.39
BFE	Brorfelde	52.14	89.54
HAD	Hartland	48.12	74.79
BEL	Belsk	47.84	96.09
CLF	Chambon La Foret	44.12	79.35
FUR	Furstenfeldbruk	44.01	86.91
TAM	Tamanrasset	6.81	78.31
MBO	Mbour	0.11	57.85

[a]Data taken from the nearby LOV station prior to 2003.

definition is also suitable for studies considering GICs, for which field rotations may be significant (e.g., Beggan, 2015).

2.2. Sudden Commencements

We utilize an independent catalog of SCs, maintained by the International Service on Rapid Magnetic Variations (part of the International Service of Geomagnetic Indices), based at Ebre Observatory. These SC intervals have been identified based on inspection of the data from five low-latitude observatories (Curto et al., 2007), spaced around the globe in longitude as close to the magnetic equator as possible. The yearly catalogs can be found at http://www.obsebre.es/en/rapid/. We use the catalogs for the years 1996–2016 (inclusive). During this interval a total of 380 SCs were recorded which, given each SC is approximately 5 min in duration, cumulatively corresponds to ~1,900 min of data. While the start and end of the SC magnetic signatures were determined manually, the average ~5 min interval corresponds closely with the response time of the magnetopause to a solar wind shock (Freeman & Farrugia, 1998; Freeman et al., 1995).

SCs may be classified retrospectively based on whether a geomagnetic storm is observed in the hours following the SC. If a storm is observed then it is classed as a SSC, if not then it is termed a Sudden Impulse (SI). Often such a classification is evaluated using the minimum observed values of the Dst or Sym-H indices (e.g., Curto et al., 2007; Fiori et al., 2014; Gonzalez et al., 1994; Joselyn & Tsurutani, 1990; Turner et al., 2015). In this work we designate an SC as an SSC if Sym-H drops below −50 nT in the 24 h following the SC, and otherwise designate it as an SI. In total, 215 events meet the criteria and are classed as SSCs, which leaves 165 SIs. Historically, the distinction has also been made by considering whether the magnetic "rhythm" at the station changed character (e.g., Mayaud, 1973); however, this is more difficult to perform in an automated and reproducible fashion, and so has not been applied. This scheme follows that used by Smith et al. (2019), and ensures that the results are directly comparable with that earlier study.

3. Results

3.1. Assessing the Probability Density Functions of R

Figure 2 shows Probability Density Functions (PDFs) of R for the 12 stations included in this study. Figure 2a shows the PDFs of R for the full data set (1996–2016) and Figure 2b shows the PDF of R during SCs. Figure 2c shows the ratio of the PDFs observed during SCs to the PDFs from the complete data set, showing the relative likelihood of a level of R during SCs compared to the data set as a whole. The PDFs are binned using the method of Freeman et al. (2019), while the color indicates the magnetic latitude of the observatory.

For the full interval (Figure 2a), the PDFs show a clear ordering, with PDFs from stations at higher latitudes (i.e., those that are toward the red end of the color scale) showing higher probability densities at larger R when compared with those at lower geomagnetic latitudes (i.e., those toward the blue end of the color scale). This shift is most dramatic at mid to high latitudes, that is, for stations with geomagnetic latitudes greater then ~55°. For example, at an R of 10 nT min^{-1} the difference between the PDFs of stations near the magnetic equator (e.g., MBO) and those at ~55° (e.g., LER) is approximately an order of magnitude, showing that R of this level is ~10 times more common at the higher latitude station. Meanwhile, the difference between stations at ~55° and those at ~65° (e.g., ABK) is also an order of magnitude, despite a much smaller latitudinal difference. This highlights the region at which the phenomena related to the auroral currents begin to exert a greater influence on the rate of change of the field (e.g., Rogers et al., 2020).

When we compare the PDFs obtained during SC intervals (Figure 2b) we find that they are shifted toward larger R, as seen for the entire data set (seen in Figure 2a). Again, this effect appears to be more pronounced

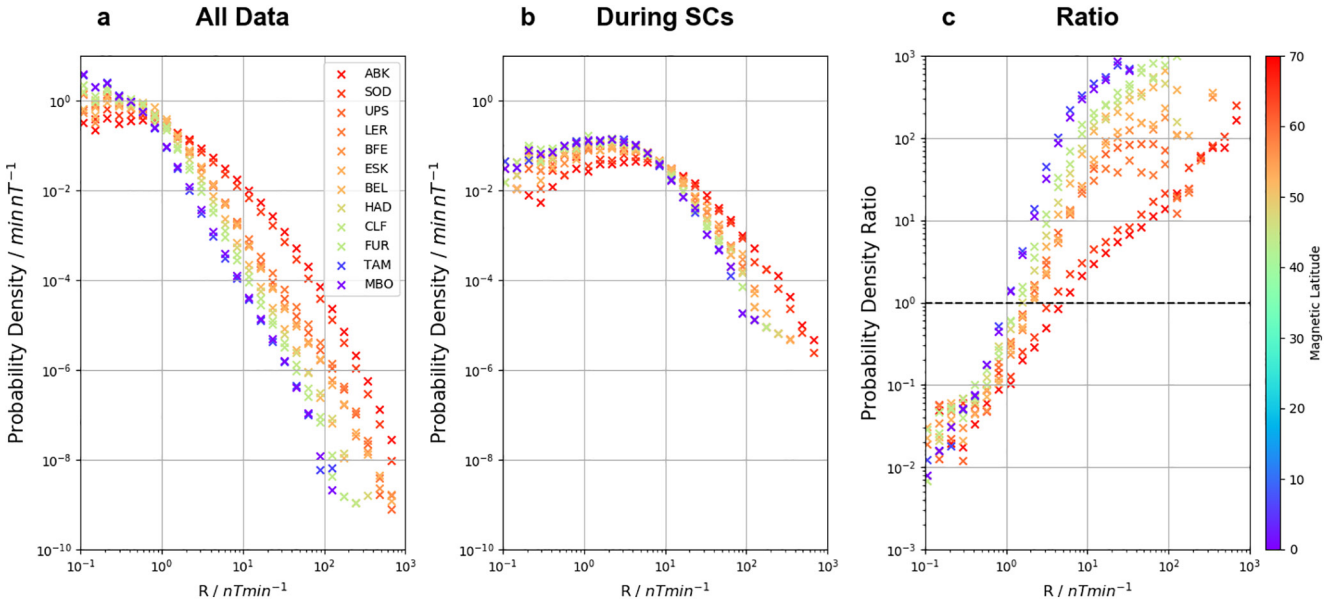

Figure 2. PDFs of R between 1996 and 2016 for the 12 magnetometer stations in Figure 1 and Table 1 (a), PDFs of R during 380 SC intervals for the same stations (b), and the ratio between the PDF during SCs and at all times (c). The color of the PDF is given by the magnetic latitude of the magnetometer station. PDF, Probability Density Functions.

at higher latitudes, with a greater shift to larger values of R. As the SCs included are identical between stations, this suggests that larger values of R are observed at higher latitude stations during the same SC event, reflecting a form of high latitude enhancement (e.g., Fiori et al., 2014).

The ratio of the PDFs from the SCs to the PDFs from the entire data set for each station are shown in Figure 2c. The dashed horizontal line indicates a ratio of 1. These ratios show that rates of change smaller than ~1–10 nT min^{-1} are less likely during SCs than at a randomly selected interval, while R larger than ~1–10 nT min^{-1} are more likely to be observed. This transition was previously noted in a study of the subset of data from the UK based stations (Smith et al., 2019). The transition can be seen to vary with latitude. Lower latitude stations (e.g., below 50°) show this transition at values of $R \sim 1$ nT min^{-1}, while higher latitude stations see it closer to 10 nT min^{-1}. It is also noteworthy that the ratio of the PDFs at significant R (e.g., $R > 10$ nT min^{-1}) is much larger at lower latitude stations. For example, at low latitudes an R of 30 nT min^{-1} is ~700 times more likely to be observed during an SC than at any randomly selected interval. In contrast, at the highest latitude station (e.g., ABK), observations of $R = 30$ nT min^{-1} are only approximately seven times more likely during SCs. Therefore, while SCs are associated with larger R at higher latitudes, SCs are more likely to be associated with unusually large R at lower latitudes.

3.2. The Contribution of SCs

Smith et al. (2019) found that around 8% of observations of $R \geq \sim 50$ nT min^{-1} were directly attributable to SCs for the HAD station at a magnetic latitude of 47.37°. To explore how this changes with latitude, Figure 3a shows the percentage of data exceeding prescribed levels of R that can be directly related to SCs. The percentages are plotted for each of the 12 stations, with the color once again indicating the geomagnetic latitude of the station. It is clear from Figure 3a that SCs become responsible for an increasing percentage of extreme variation as the geomagnetic latitude of the station reduces toward the equator. Above a level of ~60 nT min^{-1} up to 40% of the observations are related directly to SCs at the lowest latitude stations. As latitude increases to approximately 45° this percentage decreases to 10%–20%. For the stations at higher latitudes, for example, above ~60°, less than 1% of data above an R of 10s of nT min^{-1} is attributable to SCs. This again highlights the importance and significance of other phenomena at these latitudes.

Figures 3b and 3c are plotted in the same format as Figure 3a, however, the SCs have been split into those classed as SSCs (Figure 3b) and SIs (Figure 3c). This classification has been performed on the basis of the

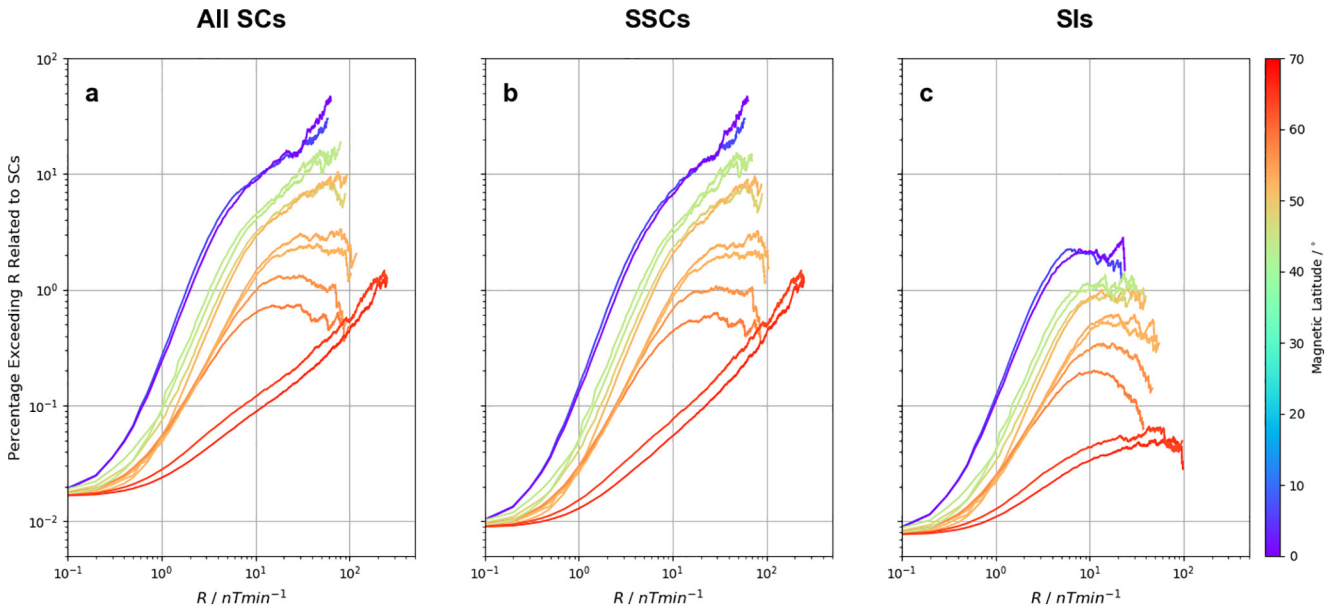

Figure 3. The percentage of data (1996–2016) exceeding a given level of R that is related to SCs. The results for each of the 12 stations are plotted, with the color representing the magnetic latitude of the station. The curves are shown for all 380 SCs (a), 215 SSCs (b), and 165 SIs (c), as defined in Section 2.2. The lines/percentages for each station are truncated where less than five positive instances remain in order to remove variability at large R related to a small number of statistics. SC, Sudden Commencements; SSC, Storm Sudden Commencement; SI, Sudden Impulse.

Sym-H index in the 24 h that follow the SC (see Section 2.2). It can be seen that Figure 3b closely resembles Figure 3a, such that the majority of the large rates of change can be attributed to the 215 SSCs. Figure 3c on the other hand, displaying the rates of change associated with SIs, shows a similar pattern but the percentages are about an order of magnitude lower. SIs can be seen to account for less than 2% of observations of elevated R even at the lowest latitudes. This suggests that the interplanetary shocks that create the most significant initial ground response are more likely to lead to further global magnetospheric activity, that is, a geomagnetic storm.

3.2.1. Quantifying the Contribution Above 50 nT min^{-1}

We now look to quantitatively evaluate how the fraction of large R attributable to SCs changes with latitude, and how the days that follow the SC contribute to that fraction of R. Figure 4 shows how the percentage of data above 50 nT min^{-1} related to SCs varies as a function of magnetic latitude. Effectively, Figure 4 shows vertical slices through Figure 3 at R = 50 nT min^{-1}. The 50 nT min^{-1} threshold has been selected as it represents a large rate of change at all stations, yet retaining sufficient data at all latitudes. The impact of changing this threshold will be assessed in Section 3.2.2. Inspecting the top row of Figure 4 we see that an increasing percentage of data above 50 nT min^{-1} is attributable to SCs as magnetic latitude decreases, leading to a maximum of ∼32% at the lowest latitude station. Specifically, the 50 nT min^{-1} threshold was broken on 12 occasions during SCs (during 11 separate events), out of a total of 38 total intervals above 50 nT min^{-1}. Meanwhile, above a geomagnetic latitude of approximately 50° the equivalent percentage is very small (≤1%). Comparing SSCs and SIs (Figures 4b and 4c (i)) we again find that SIs are responsible for less than 1% of instances of R exceeding 50 nT min^{-1} at any latitude.

When we include the data obtained in the 24 h that follows an SC (Figure 4a (ii)) we see that below a latitude of 60° about 75% of R exceeding 50 nT min^{-1} occurs during this interval, rising to 80%−90% at the lowest latitude stations. Above a magnetic latitude of 60° this percentage is below 50%. As with the data from the SCs themselves, when we subdivide the SCs by type (Figures 4b (ii) and 4c (ii)) we find that the period 24 h following SIs accounts for less than 1% of the R exceeding 50 nT min^{-1}.

Including the second and third days after the SCs increases the percentage of $R \geq 50$ nT min^{-1} that can be explained incrementally, by approximately 10%–20% per additional day included (e.g., moving from Figure 4a (iii–iv)). For stations at latitudes lower than 60°, 90%–100% of all R exceeding 50 nT min^{-1} occurred within

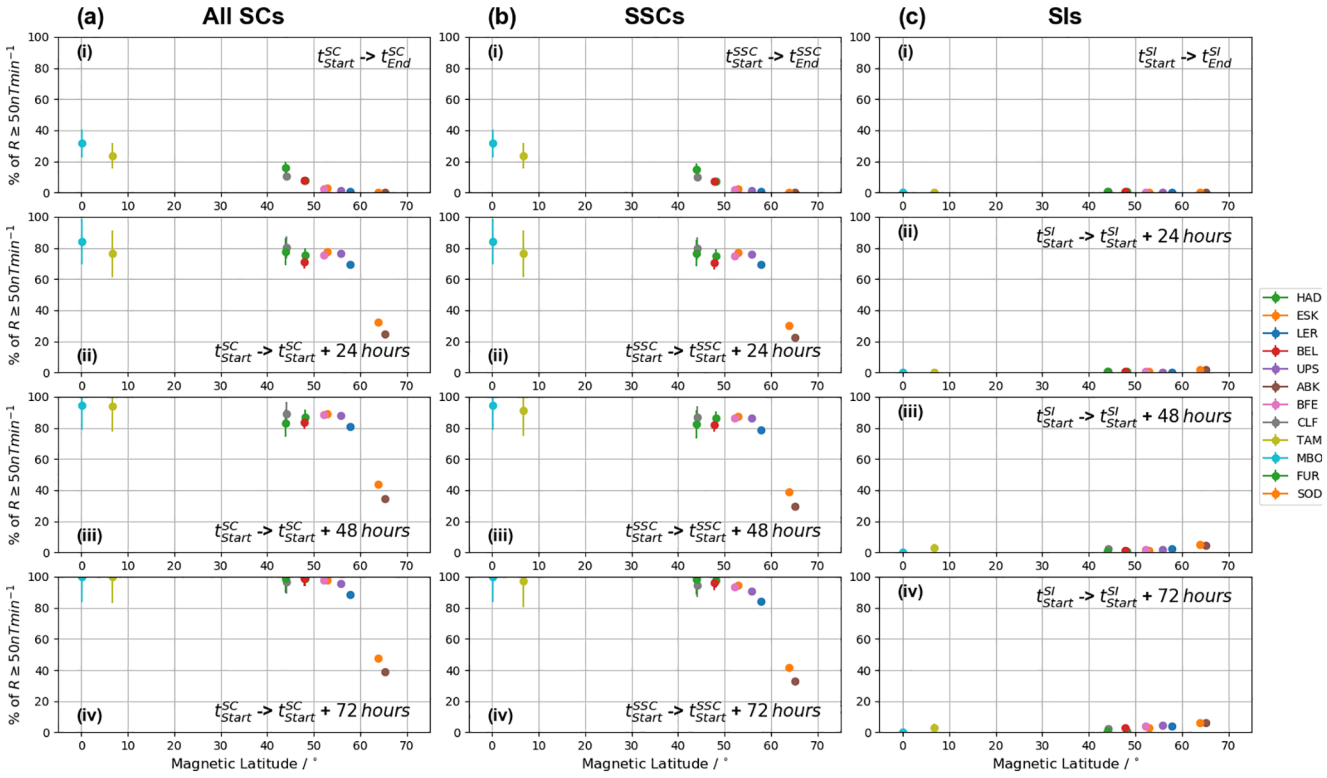

Figure 4. The percentage of observations of $R \geq 50$ nT min^{-1} that can be related to SCs as a function of magnetic latitude. The columns are plotted for (a) all 380 SCs, (b) 215 SSCs, and (c) 165 SIs. The rows represent the data obtained during the SCs themselves (i), then the data inclusive of 24, 48, and 72 h following the SC (ii, iii, and iv, respectively).

3 days of an SC. In contrast, above 60° the percentage is still below ∼50%. Mirroring the results in Figure 3, when splitting the SCs into SSCs and SIs, we find that SSC related intervals account for almost all of the $R \geq 50$ nT min^{-1}, while SIs and the related intervals account for <5% at all latitudes.

We note that 87 of the SCs occur within the 3-day interval following a previous SC. For these events, the rates of change of the field are included in the statistics of the most recent SC, and are not double-counted.

3.2.2. Evaluating the Contribution as a Function of Threshold

In the above we considered the contribution of SCs to rates of change above a fixed threshold of 50 nT min^{-1}. We now examine how adjusting this R threshold impacts how the contribution of SCs changes with latitude. Figures 5a and 5b show how this percentage varies for SCs and SCs + 1 day (i.e., in the first 24 h), respectively. Panels (i– vii) in Figure 5 show the results for thresholds between 10 to 70 nT min^{-1}, in increments of 10 nT min^{-1}. First, considering just the data during SCs themselves (Figure 5a), as the threshold increases we see that the fraction of R attributable to SCs increases. This trend can also be seen in Figure 3. Above 10 nT min^{-1} (Figure 5a (i)) at the most equatorial station ∼10% of the data is directly related to SCs, while by the time the threshold is set to 70 nT min^{-1} this increases to around 35%. However, it is also clear that this increase in percentage is mostly concentrated at lower latitudes, and that above ∼50° geomagnetic latitude the increase is relatively minor.

When we include the data that occurred in the day that follows an SC, that is, inspecting Figure 5b (i–vii), we find that the percentage attributable to this SC related interval is relatively constant with increasing threshold. Over a threshold of ∼20 nT min^{-1}, it plateaus at approximately 70%–80% for most latitudes. Above 60° however, a smaller percentage is attributable to SCs and the following 24 h of observations. For these high latitude stations, above 10 nT min^{-1} around 15% of data is explained, which increases to around 25%–30% at levels above 70 nT min^{-1}.

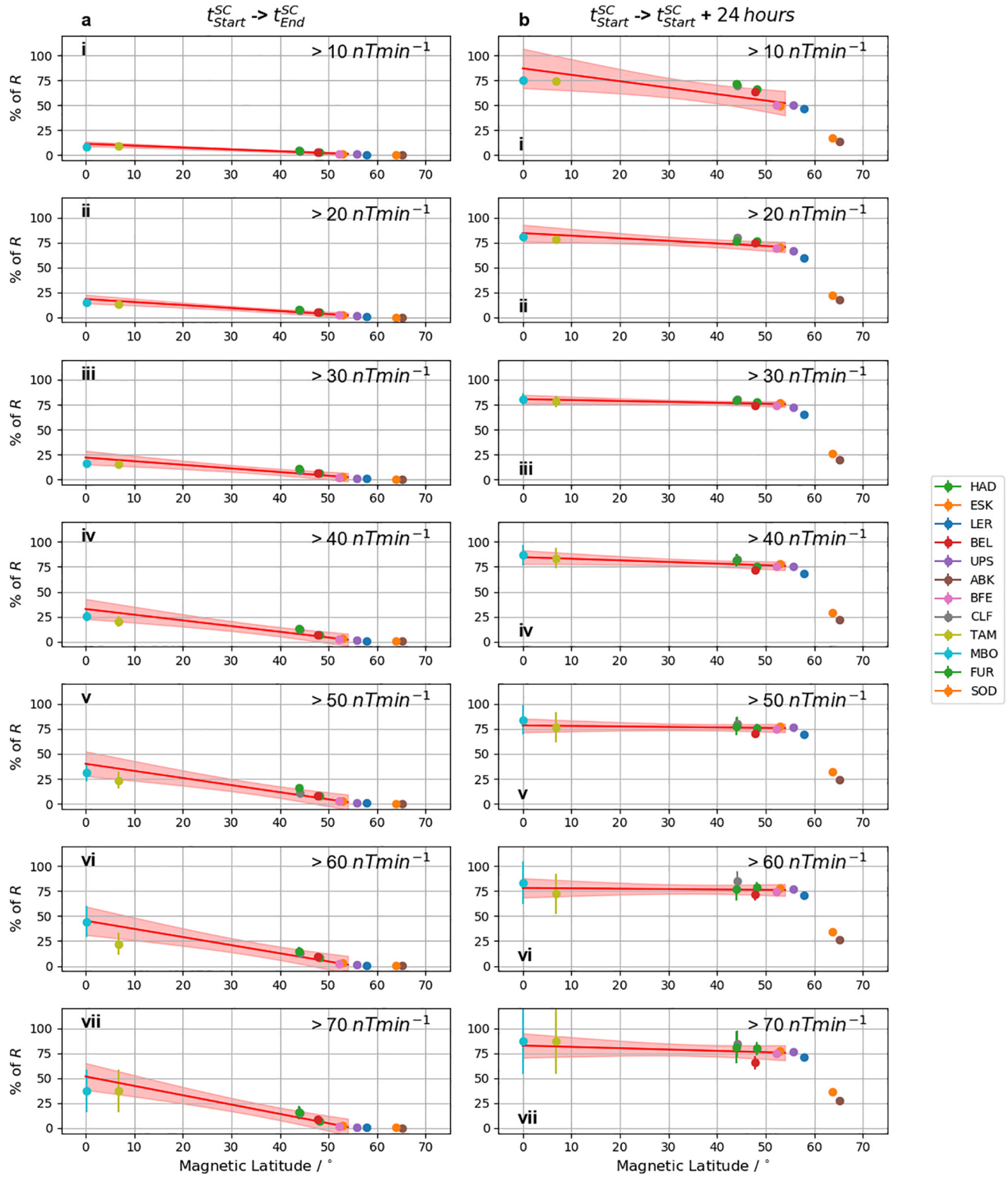

Figure 5. The fraction of data exceeding given values of R that can be related to SCs as a function of magnetic latitude, for increasing thresholds of R in panels (i–iv). The threshold ranges from 10 nT min^{-1} (i) to 70 nT min^{-1} (vii) in steps of 10 nT min^{-1}. The columns are plotted for all 380 SCs (a) and all 380 SCs including the 24 h that follow (b). The red line indicates the results of a linear fit to stations at less than 55° magnetic latitude. The red shaded region indicates the 95% confidence interval from the linear fitting procedure.

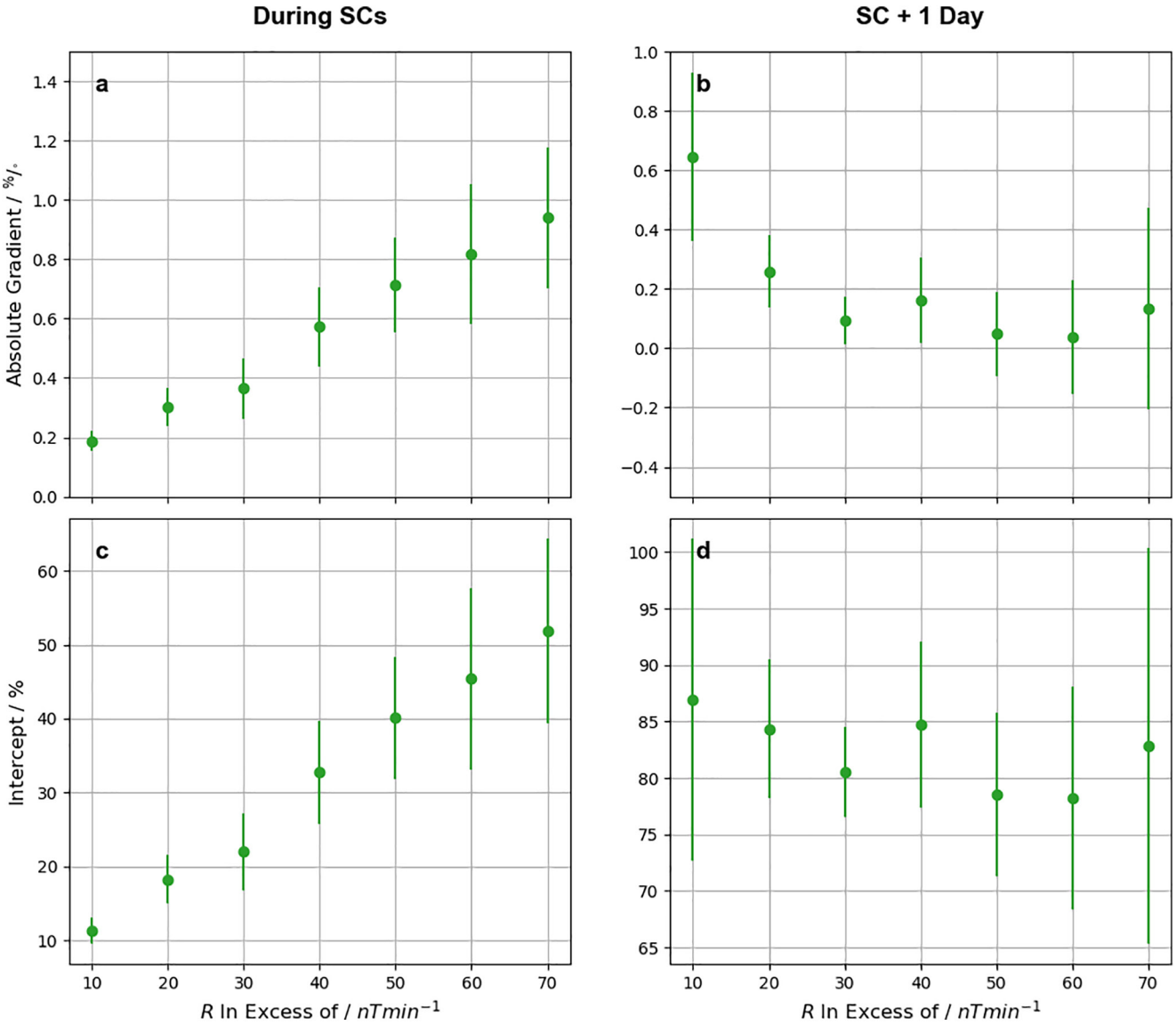

Figure 6. The results of the linear fits to Figure 5, below a latitude of 55°. The absolute value of the linear best fit gradient for SCs and SCs plus 1 day, respectively (a and b). The value of the intercept at the magnetic equator, once more for SCs and SCs plus 1 day (c) and (d). The error bars indicate the 1σ uncertainty in the least squares fit, calculated from the covariance matrix.

The red lines in Figure 5 represent simple linear fits to the results from stations below 55° magnetic latitude. The fitting limit of 55° was determined manually from inspection, where stations above this latitude have results that appear significantly different. This linear fit can be seen to well to capture most of the trends, particularly in Figure 5a (during SCs). The parameters of these empirical fits are shown in Figure 6.

In Figure 6a, which shows the results for the SC intervals, we see that the gradient of the fit increases as the threshold of R increases. Further, this same pattern is seen in the intercept (Figure 6c), which is equivalent to the equatorial projection of the percentage contribution of SCs, assuming a linear fit to the stations below 55°. This equatorial percentage increases from ~10% at a limit of 10 nT min^{-1}, exceeding a fraction of ~40% above an $R \sim 50$ nT min^{-1}, albeit with considerable uncertainty at the higher thresholds. This combination of increasing gradient and intercept with threshold suggest that while SCs do become more important at higher thresholds at all latitudes, this increase is greatest at the lowest latitudes.

Considering the results for SCs and the day that follows, Figures 4b and 4d, we see that the gradient decreases and flattens to zero as the R threshold increases, while the intercept remains relatively constant. Nonetheless, the intercept appears between 75% and 90%, suggesting that, within uncertainties the vast majority of $R \geq 10$ nT min^{-1} at low latitudes is found within a day of an SC. Further, due to the small gradients obtained, this result is widely applicable to locations with magnetic latitudes below 55°.

4. Discussion

In this work we have evaluated the contribution of SCs to large rates of change of the ground magnetic field as a function of latitude, using an array of 12 magnetometer stations across Europe and North Africa. Our results show that while SCs are larger at higher geomagnetic latitudes, they form a larger fraction of extreme magnetic field variability at lower latitudes. Further, only SSC type events cause significant magnetic field variability and below 60° magnetic latitude the 3 days that follow an SSC contribute the vast majority of R above 50 nT min^{-1}.

4.1. Latitudinal Variation of SC Risk

We examined how the PDFs of R change with geomagnetic latitude (Figure 2), comparing and contrasting the complete data set with that obtained during SC-related intervals. We showed that higher latitude stations show PDFs that are shifted toward larger values of R, both during SCs and in the full data set. SCs have been observed to present with larger rates of change of the field at higher magnetic latitudes, and this has been linked to ionospheric current systems that are only generated at such locations (e.g., Araki, 1994; Fiori et al., 2014). While the magnitude of SCs is lower closer to equatorial latitudes, we also showed that they represent intervals during which rates of change of around 30 nT min^{-1} are up to 700 times more likely that during any random interval. This relative likelihood is smaller at higher latitudes, being of the order of 10 times more likely. As the rate of change (R) increases, SCs contribute an even greater percentage of the data at low latitudes. This demonstrates how at lower latitudes there are fewer phenomena that can generate large rates of change of the field. Meanwhile, at higher latitudes other magnetospheric processes, such as storms, substorms, and convection can be inferred to control the majority of significant R (e.g., Freeman et al., 2019).

We have also shown that the importance of the period that follows SCs is considerable, with the first day post-SC accounting for around 85% of variability exceeding 20 nT min^{-1}, below a latitude of 55°. While this does not change significantly as the latitude increases from the equator, there is a considerable jump at around 55°–60° magnetic latitude, above which SCs and the days that follow only contribute a dramatically ∼30% of the large values of R, at all thresholds tested. This corresponds to the region in which the auroral currents most often reside (Rogers et al., 2020; Thomson et al., 2011). This is not to say that SCs do not have an impact at these latitudes, but they are a part of a plethora of geomagnetic activity that can result in large magnetic perturbations at the ground.

4.2. Link to GICs: Comparison With New Zealand

Large GICs have been directly measured during SCs and during magnetospheric activity that follows (e.g., Pulkkinen et al., 2005; Rodger et al., 2017). Clilverd et al. (2018) performed a detailed study of the September 2017 geomagnetic storm, using observations of the local magnetic field variability and GICs in New Zealand and noted that each of the two interplanetary shock impacts in the interval studied were associated with enhanced variability in the field and GICs. They also found that both of these SCs were followed a few hours later by a second interval of elevated field variability and considerable GIC probably associated with substorms. Our study corroborates these results and places them in the context of observations from a large historical data set of ground magnetic field rates of change, showing that the largest amplitude variations occur within the period following SSCs. However, we lack direct and contemporaneous observations of GICs for the European and North African locations included in the current study. It is therefore instructive to compare our statistical geomagnetic field variability results from the northern hemisphere with New Zealand, where direct GIC measurements are available and strong correlations between SCs and related magnetospheric activity and GICs have been observed.

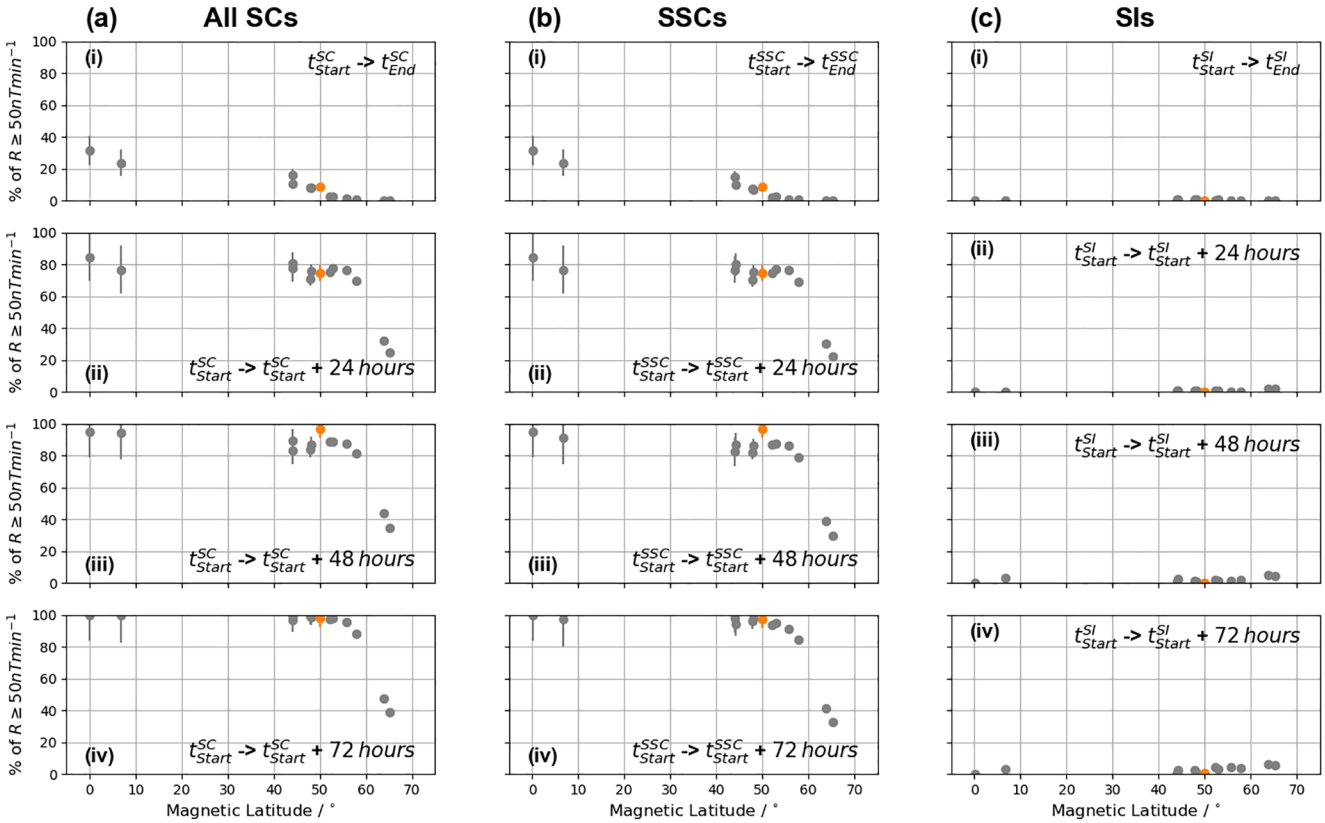

Figure 7. The percentage of $R \geq 50$ nT min^{-1} that can be related to SCs as a function of magnetic latitude. The format is as in Figure 4, with the 12 stations in Table 1 shown in gray and the EYR station in orange.

Figure 7 shows the percentage of data for which $R \geq 50$ nT min^{-1} that is associated with SCs as a function of magnetic latitude. The format is the same as in Figure 4, but with the 12 stations originally included in this study now plotted in gray. The EYR INTERMAGNET station, located at Eyrewell in New Zealand at a magnetic latitude of −50° and longitude of −103.64°, is included in orange at its conjugate latitude.

The results from EYR are consistent with the previously noted trends from the northern hemisphere stations. We note that the original station selection process (Section 2) required that the stations were as close together in longitude as possible, in order to mitigate any local time effects. This consistency between the north and south results indicates that the local time differences that prompted the longitudinal constraints imposed in our station selection are relatively minor over the long statistical time period considered in this work. This suggests that the results we report are likely more broadly applicable rather than being restricted to the longitude range of stations shown in Figure 1. This also suggests that the close associations noted between GICs and SCs (and following intervals) in New Zealand may also be present in other locations if such direct GIC measurements were available. However, we note that while the statistical analysis of the rate of change of the magnetic field is consistent between these locations, the relationship between magnetic fluctuations and GIC depends strongly on the orientation of the power network, its internal connectivity and resistivity, and local geology (e.g., Beggan, 2015; Divett et al., 2018; Thomson et al., 2005).

It is also interesting to note that although we have considered the initial SC impact and the magnetospheric activity in the days that follow as a whole (e.g., storms and substorms), distinct phenomena may have slightly different implications for power networks. Part of this will be due to the orientation of the variability, for example, SCs are predominantly in the northward direction which would couple differently to a given power network than an east-west deflection. Second, different phenomena will operate over different timescales, which may present a different hazard to a given system (e.g., Clilverd et al., 2020). The different effects of the distinct phenomena were noted by Clilverd et al. (2018), who found that while SSCs and later periods both resulted in the generation of significant GICs in the power network, only the longer lasting post-SC

intervals were related to the generation of harmonics in the power network. This kind of consideration would be of key importance to the use of forecasts of SCs in the operation of power networks.

It is also important to note that this study has concerned the results obtained with one-minute resolution magnetic field data, which have been shown to correlate well with observed GICs (e.g., Mac Manus et al., 2017; Rodger et al., 2017). Yet SCs often represent very fast magnetic fluctuations that may not be adequately captured by one-minute resolution data (e.g., Araki, 2014). For this reason, it may be that SCs are more important when the rates of change of higher resolution magnetic field data are considered. However, we note that due to smoothing effects from the local ground conductivity and network inductance, high frequency magnetic fluctuations do not necessarily translate directly to significant GICs (e.g., Clilverd et al., 2020; Divett et al., 2018).

4.3. Forecasting Large Geomagnetic Field Fluctuations

From the perspective of mitigating the risks posed by GICs, it is of great importance to be able to forecast intervals in which they might be generated. Until recently, there had been little success at forecasting substorms, and therefore the substorm-driven GICs with which they are associated. It had been shown that their recurrence and amplitude could be predicted statistically, but not for individual events (Freeman & Morley, 2004; Morley & Freeman, 2007). Recently, however, Maimaiti et al. (2019) showed that machine learning methods can be used to predict substorms 75% of the time. Nevertheless, the solar wind driving between substorm and non-substorm intervals showed strong similarities, testifying to the difficulty of forecasting such a phenomenon purely on the basis of the external solar wind.

Looking to forecasting other significant phenomena, approximately 75% of SCs are preceded by the observation of an interplanetary shock upstream of the Earth at L1 (Smith et al., 2020; Wang et al., 2006), providing a significant amount of warning and the opportunity to forecast the consequences of the shock. Excellent correlations have historically been observed between large geomagnetic storms and interplanetary shocks (Chao & Lepping, 1974; Gosling et al., 1991); while statistically between ∼45% and 60% of interplanetary shocks incident at the Earth being linked to geomagnetic storm activity in the days that follow (Echer & Gonzalez, 2004).

The SCs studied in this work have been broken down by whether they were followed by further significant geomagnetic activity, that is, a geomagnetic storm. Those that are can be termed an SSC, while those that are not can be called a SI (e.g., Curto et al., 2007; Joselyn & Tsurutani, 1990). Recent modeling efforts have shown good skill and reliability in distinguishing between interplanetary shocks likely to result in SSCs or SIs in advance (Smith et al., 2020). When we make such a distinction, we found that SI-type events are not related to substantial fractions of enhanced R. In contrast, the substantial fractions of enhanced R observed during the full complement of SCs (or in the days that follow) are solely due to those events that have been classed as SSCs. Therefore, being able to make this distinction would help to narrow consideration of intervals during which large R maybe observed.

Our results confirm the critically important contribution of SSCs to low-to-mid latitude magnetic field perturbations (e.g., Carter et al., 2015; Marshall et al., 2012). They suggest that for the lowest latitudes SSCs are one of the dominant processes that can generate large R, and consequently large GIC. At equatorial magnetic latitudes, the ability to forecast SSCs would allow a 24 h window to be identified which would account for over 80% of rates of change of the magnetic field greater than 70 nT min^{-1}. Meanwhile at mid latitudes, as with the preliminary work of Smith et al. (2019), we have found that the days that follow SSCs contribute strongly to values of R exceeding 50 nT min^{-1}. Over 90% of such values of R are recorded within 3 days of an SSC for stations below ∼55°–60°. Therefore, observations upstream of the Earth allow for a broad window of warning that such large R may occur in the next few days at mid-low latitudes. Such a warning could be exploited by the energy transmission industry, applying mitigation approaches over that time window.

These results also have consequences for the horizon with which large rates of the change can be forecast. Without the use of heliospheric imagery or models (e.g., Barnard et al., 2019, 2020; Davies et al., 2012, 2013; Odstrcil, 2003; Owens & Riley, 2017; Owens et al., 2020), the large rates of change of the field caused by an interplanetary shock impact (i.e., an SC) may be, at most, forecast by the travel time between the observations at L1 and the Earth's magnetopause: likely less than an hour. Therefore, at the lowest latitudes around

25%–35% of large rates of change of the field may only be forecast with a maximum of an hour lead time. On the other hand, the very large fraction of mid-low latitude rates of change observed in the days that follow an SC may be forecast with a longer lead time, though imprecisely.

At high geomagnetic latitudes, here defined to be around ∼55°–60°, the relative importance of other phenomena was shown to increase such that ≤50% of R exceeding 50 nT min^{-1} is found within 3 days of an SSC. At these latitudes it is likely that forecasting phenomena outside of geomagnetic storms such as substorms is a critical process (e.g., Maimaiti et al., 2019). Such forecasting would also provide a more precise window of warning, of the order of an hour, rather than the days provided by consideration of SSCs and related activity.

5. Summary

In this work we have assessed the contribution of SCs to large rates of change of the horizontal magnetic field (R), exploring this as a function of latitude and level of variability. In general, large rates of the change of the magnetic field would be expected to drive large GICs, which may pose a risk to the operation of power networks.

We have shown that the relative importance of SCs producing high R increases moving toward the equator, and that at the lowest latitudes during an SC magnetic fluctuations around 30 nT min^{-1} are around 700 times more likely that in any random interval. In contrast, by a latitude of ∼65° this factor drops to less than 10 times more likely.

We have shown that SCs represent over 25% of geomagnetic field fluctuations above 50 nT min^{-1} at the lowest latitudes. Again, this drops off as latitude increases to ≤1% by ∼55°. If we include the 3-days interval following an SC, we can account for greater than 90% of field fluctuations above 50 nT min^{-1} below a magnetic latitude of ∼60°. Above this latitude other phenomena that may be unrelated to SCs, such as non-storm time isolated substorms, account for the majority of magnetic perturbations.

Critically, we have also shown that the elevated values of R associated with SCs are almost entirely due to the subset of SCs that are followed by a geomagnetic storm, termed SSCs. This is observed both for the case of immediate large R, and also for the few days that follow.

This work has quantified the impact of SCs, and confirmed their significance for mid-low latitude magnetic field changes, both directly and also as an indication that significant geomagnetic activity may follow. This has important consequences for the forecasting of large rates of change of the geomagnetic field, and consequent GICs.

Acknowledgments
A. W. Smith and I. J. Rae were supported by STFC Consolidated Grant ST/S000240/1, and NERC grants NE/P017150/1 and NE/V002724/1. C. Forsyth was supported by the NERC Independent Research Fellowship NE/N014480/1, NERC grant NE/V002724/1 and STFC Consolidated Grant ST/S000240/1. C. J. Rodger was supported by the New Zealand Ministry of Business, Innovation & Employment through Endeavor Fund Research Program contract UOOX2002. M. P. Freeman was supported by NERC grants NE/P016693/1 (SWIGS) and NE/V002716/1 (SWIMMR SAGE). The analysis in this paper was performed using python, including the pandas (McKinney, 2010), numpy (Van Der Walt et al., 2011), scikit-learn (Pedregosa et al., 2011), scipy (Virtanen et al., 2020) and matplotlib (Hunter, 2007) libraries. The authors thank the involved national institutes, the INTERMAGNET network and the ISGI.

Data Availability Statement

The results presented in this study rely on data collected at magnetic observatories. We thank the national institutes that support them and INTERMAGNET for promoting high standards of magnetic observatory practice (www.intermagnet.org). The data were downloaded from https://intermagnet.github.io and are freely available there. The results presented in the paper also rely on the SC list made available by the International Service on Rapid Magnetic Variations (http://www.obsebre.es/en/rapid) and published by the Observatorio de l'Ebre in association with the International Association of Geomagnetism and Aeronomy (IAGA) and the International Service of Geomagnetic Indices (ISGI).

References

Akasofu, S.-I. (1964). The development of the auroral substorm. *Planetary and Space Science*, *12*(4), 273–282. https://doi.org/10.1016/0032-0633(64)90151-5

Akasofu, S.-I., & Chao, J. (1980). Interplanetary shock waves and magnetospheric substorms. *Planetary and Space Science*, *28*(4), 381–385. https://doi.org/10.1016/0032-0633(80)90042-2

Araki, T. (1977). Global structure of geomagnetic sudden commencements. *Planetary and Space Science*, *25*(4), 373–384. https://doi.org/10.1016/0032-0633(77)90053-8

Araki, T. (1994). A physical model of the geomagnetic sudden commencement. In M. Engebretson, K. Takahashi, & M. Scholer (Eds.), *Solar wind sources of magnetospheric ultra-low-frequency waves* (p. 183). AGU. Retrieved from https://doi.org/10.1029/GM081p0183

Araki, T. (2014). Historically largest geomagnetic sudden commencement (SC) since 1868. *Earth Planets and Space*, *66*(1), 164. https://doi.org/10.1186/s40623-014-0164-0

Araki, T., Fujitani, S., Emoto, M., Yumoto, K., Shiokawa, K., Ichinose, T., et al. (1997). Anomalous sudden commencement on March 24, 1991. *Journal of Geophysical Research*, *102*(A7), 14075–14086. https://doi.org/10.1029/96JA03637

Barnard, L., Owens, M. J., Scott, C. J., & Jones, S. R. (2019). Extracting inner heliosphere solar wind speed information from heliospheric imager observations. *Space Weather*, *17*(6), 925–938. https://doi.org/10.1029/2019SW002226

Barnard, L., Owens, M. J., Scott, C. J., & Koning, C. A. (2020). Ensemble CME modeling constrained by heliospheric imager observations. *AGU Advances*, *1*(3), e2020AV000214. https://doi.org/10.1029/2020AV000214

Bedrosian, P. A., & Love, J. J. (2015). Mapping geoelectric fields during magnetic storms: Synthetic analysis of empirical United States impedances. *Geophysical Research Letters*, *42*(23), 10160–10170. https://doi.org/10.1002/2015GL066636

Beggan, C. D. (2015). Sensitivity of geomagnetically induced currents to varying auroral electrojet and conductivity models. *Earth. Planets and Space*, *67*(1), 24. https://doi.org/10.1186/s40623-014-0168-9

Beland, J., & Small, K. (2004). Space weather effects on power transmission systems: The cases of Hydro-Quebec and transpower New Zealand Ltd (Proceedings Paper). In I. Daglis (Ed.), *Effects of space weather on technology infrastructure* (Vol. 176, pp. 287–299). Springer.

Borovsky, J. E., & Denton, M. H. (2006). Differences between CME driven storms and CIR driven storms. *Journal of Geophysical Research*, *111*(A7), A07S08. https://doi.org/10.1029/2005JA011447

Boteler, D. H., Pirjola, R. J., & Nevanlinna, H. (1998). The effects of geomagnetic disturbances on electrical systems at the Earth's surface. *Advances in Space Research*, *22*(1), 17–27. https://doi.org/10.1016/S0273-1177(97)01096-X

Campbell, W. H. (1980). Observation of electric currents in the Alaska oil pipeline resulting from auroral electrojet current sources. *Geophysical Journal International*, *61*(2), 437–449. https://doi.org/10.1111/j.1365-246X.1980.tb04325.x

Carter, B. A., Pradipta, R., Zhang, K., Yizengaw, E., Halford, A. J., & Norman, R. (2015). Interplanetary shocks and the resulting geomagnetically induced currents at the equator. *Geophysical Research Letters*, *42*(16), 6554–6559. https://doi.org/10.1002/2015gl065060

Chao, J. K., & Lepping, R. P. (1974). A correlative study of SSC's, interplanetary shocks, and solar activity. *Journal of Geophysical Research*, *79*(13), 1799–1807. https://doi.org/10.1029/JA079i013p01799

Chree, C. (1925). The times of "Sudden Commencements" (S.C.s) of magnetic storms: Observation and theory. *Proceedings of the Physical Society of London*, *38*(1), 35–46. https://doi.org/10.1088/1478-7814/38/1/305

Clilverd, M. A., Rodger, C. J., Brundell, J. B., Dalzell, M., Martin, I., Mac Manus, D. H., et al. (2018). Long-lasting geomagnetically induced currents and harmonic distortion observed in New Zealand during the 7–8 September 2017 disturbed period. *Space Weather*, *16*(6), 704–717. https://doi.org/10.1029/2018SW001822

Clilverd, M. A., Rodger, C. J., Brundell, J. B., Dalzell, M., Martin, I., Mac Manus, D. H., & Thomson, N. R. (2020). Geomagnetically induced currents and harmonic distortion: High time resolution case studies. *Space Weather*, *18*, e2020SW002594. https://doi.org/10.1029/2020SW002594

Committee on the Peaceful Uses of Outer Space (COPUOS). (2017). *Thematic priority 4. International framework for space weather services (Tech. Rep.).*

Coxon, J. C., Shore, R. M., Freeman, M. P., Fear, R. C., Browett, S. D., Smith, A. W., et al. (2019). Timescales of Birkeland currents driven by the IMF. *Geophysical Research Letters*, *46*(14), 7893–7901. https://doi.org/10.1029/2018GL081658

Curto, J. J., Araki, T., & Alberca, L. F. (2007). Evolution of the concept of sudden storm commencements and their operative identification. *Earth Planets and Space*, *59*(11), i–xii. https://doi.org/10.1186/BF03352059

Davies, J. A., Harrison, R. A., Perry, C. H., Möstl, C., Lugaz, N., Rollett, T., et al. (2012). A self-similar expansion model for use in solar wind transient propagation studies. *The Astrophysical Journal*, *750*(1), 23. https://doi.org/10.1088/0004-637X/750/1/23

Davies, J. A., Perry, C. H., Trines, R. M. G. M., Harrison, R. A., Lugaz, N., Möstl, C., et al. (2013). Establishing a stereoscopic technique for determining the kinematic properties of solar wind transients based on a generalized self-similarly expanding circular geometry. *The Astrophysical Journal*, *777*(2), 167. https://doi.org/10.1088/0004-637X/777/2/167

Dimmock, A., Rosenqvist, L., Hall, J., Viljanen, A., Yordanova, E., Honkonen, I., et al. (2019). The GIC and geomagnetic response over Fennoscandia to the 7–8 September 2017 geomagnetic storm. *Space Weather*, *17*, 2018SW002132. https://doi.org/10.1029/2018SW002132

Dimmock, A., Rosenqvist, L., Welling, D., Viljanen, A., Honkonen, I., Boynton, R. J., & Yordanova, E. (2020). On the regional variability of dB/dt and its significance to GIC. *Space Weather*, *18*, e2020SW002497. https://doi.org/10.1029/2020SW002497

Divett, T., Richardson, G. S., Beggan, C. D., Rodger, C. J., Boteler, D. H., Ingham, M., et al. (2018). Transformer-level modeling of geomagnetically induced currents in New Zealand's South Island. *Space Weather*, *16*(6), 718–735. https://doi.org/10.1029/2018SW001814

Eastwood, J. P., Hapgood, M. A., Biffis, E., Benedetti, D., Bisi, M. M., Green, L., et al. (2018). Quantifying the economic value of space weather forecasting for power grids: An exploratory study. *Space Weather*, *16*(12), 2052–2067. https://doi.org/10.1029/2018SW002003

Echer, E., & Gonzalez, W. D. (2004). Geoeffectiveness of interplanetary shocks, magnetic clouds, sector boundary crossings and their combined occurrence. *Geophysical Research Letters*, *31*(9), L09808. https://doi.org/10.1029/2003GL019199

Engebretson, M. J., Pilipenko, V. A., Steinmetz, E. S., Moldwin, M. B., Connors, M. G., Boteler, D. H., et al. (2021). Nighttime magnetic perturbation events observed in Arctic Canada: 3. Occurrence and amplitude as functions of magnetic latitude, local time, and magnetic disturbance indices. *Space Weather*, *19*, e2020SW002526. https://doi.org/10.1029/2020SW002526

Fiori, R. A. D., Boteler, D. H., & Gillies, D. M. (2014). Assessment of GIC risk due to geomagnetic sudden commencements and identification of the current systems responsible. *Space Weather*, *12*(1), 76–91. https://doi.org/10.1002/2013SW000967

Forsyth, C., Rae, I. J., Coxon, J. C., Freeman, M. P., Jackman, C. M., Gjerloev, J., & Fazakerley, A. N. (2015). A new technique for determining substorm onsets and phases from indices of the electrojet (SOPHIE). *Journal of Geophysical Research: Space Physics*, *120*(12), 10592–10606. https://doi.org/10.1002/2015JA021343

Forsyth, C., Shortt, M., Coxon, J. C., Rae, I. J., Freeman, M. P., Kalmoni, N. M. E., et al. (2018). Seasonal and temporal variations of field-aligned currents and ground magnetic deflections during substorms. *Journal of Geophysical Research: Space Physics*, *123*(4), 2696–2713. https://doi.org/10.1002/2017JA025136

Freeman, M. P., & Farrugia, C. J. (1998). Magnetopause motions in a Newton-Busemann approach. In *Polar cap boundary phenomena* (pp. 15–26). Springer. https://doi.org/10.1007/978-94-011-5214-3_2

Freeman, M. P., Forsyth, C., & Rae, I. J. (2019). The influence of substorms on extreme rates of change of the surface horizontal magnetic field in the U.K. *Space Weather*, *17*, 827–844. https://doi.org/10.1029/2018SW002148

Freeman, M. P., Freeman, N. C., & Farrugia, C. J. (1995). A linear perturbation analysis of magnetopause motion in the Newton-Busemann limit. *Annales Geophysicae*, *13*(9), 907–918. https://doi.org/10.1007/s00585-995-0907-0

Freeman, M. P., & Morley, S. K. (2004). A minimal substorm model that explains the observed statistical distribution of times between substorms. *Geophysical Research Letters*, *31*(12), L12807. https://doi.org/10.1029/2004GL019989

Gonzalez, W. D., Joselyn, J. A., Kamide, Y., Kroehl, H. W., Ros, G., Tsuru, B. T., & Vasyliunas, V. M. (1994). What is a geomagnetic storm? *Journal of Geophysical Research: Space Physics*, *99*(A4), 5771–5792. https://doi.org/10.1029/93JA02867

Gosling, J. T., McComas, D. J., Phillips, J. L., & Bame, S. J. (1991). Geomagnetic activity associated with earth passage of interplanetary shock disturbances and coronal mass ejections. *Journal of Geophysical Research*, *96*(A5), 7831. https://doi.org/10.1029/91JA00316

Huang, C.-S., Le, G., & Reeves, G. D. (2004). Periodic magnetospheric substorms during fluctuating interplanetary magnetic field. *Geophysical Research Letters*, *31*(14), L14801. https://doi.org/10.1029/2004GL020180

Hübert, J., Beggan, C. D., Richardson, G. S., Martyn, T., & Thomson, A. W. P. (2020). Differential magnetometer measurements of geomagnetically induced currents in a complex high voltage network. *Space Weather*, *18*(4). https://doi.org/10.1029/2019SW002421

Hunter, J. D. (2007). Matplotlib: A 2D graphics environment. *Computing in Science & Engineering*, *9*(3), 90–95. https://doi.org/10.1109/MCSE.2007.55

Joselyn, J. A., & Tsurutani, B. T. (1990). Geomagnetic sudden impulses and storm sudden commencements: A note on terminology. *Eos, Transactions American Geophysical Union*, *71*(47), 1808. https://doi.org/10.1029/90EO00350

Kappenman, J. G. (1996). Geomagnetic storms and their impact on power systems. *IEEE Power Engineering Review*, *16*(5), 5. https://doi.org/10.1109/MPER.1996.491910

Kappenman, J. G. (2003). Storm sudden commencement events and the associated geomagnetically induced current risks to ground-based systems at low-latitude and midlatitude locations. *Space Weather*, *1*(3), 1016. https://doi.org/10.1029/2003SW000009

Kappenman, J. G., & Albertson, D. (1990). Bracing for the geomagnetic storms. *IEEE Spectrum*, *27*(3), 27–33. https://doi.org/10.1109/6.48847

Kilpua, E., Lugaz, N., Mays, M. L., & Temmer, M. (2019). Forecasting the structure and orientation of earthbound coronal mass ejections. *Space Weather*, *17*(4), 498–526. https://doi.org/10.1029/2018SW001944

Kokubun, S., McPherron, R. L., & Russell, C. T. (1977). Triggering of substorms by solar wind discontinuities. *Journal of Geophysical Research*, *82*(1), 74–86. https://doi.org/10.1029/JA082i001p00074

Lee, D.-Y., Lyons, L. R., Kim, K. C., Baek, J.-H., Kim, K.-H., Kim, H.-J., et al. (2006). Repetitive substorms caused by Alfvénic waves of the interplanetary magnetic field during high-speed solar wind streams. *Journal of Geophysical Research*, *111*(A12), A12214. https://doi.org/10.1029/2006JA011685

Lühr, H., Schlegel, K., Araki, T., Rother, M., & Förster, M. (2009). Night-time sudden commencements observed by CHAMP and ground-based magnetometers and their relationship to solar wind parameters. *Annales Geophysicae*, *27*(5), 1897–1907. https://doi.org/10.5194/angeo-27-1897-2009

Mac Manus, D. H., Rodger, C. J., Dalzell, M., Thomson, A. W. P., Clilverd, M. A., Petersen, T., & Divett, T. (2017). Long-term geomagnetically induced current observations in New Zealand: Earth return corrections and geomagnetic field driver. *Space Weather*, *15*(8), 1020–1038. https://doi.org/10.1002/2017SW001635

Maimaiti, M., Kunduri, B., Ruohoniemi, J. M., Baker, J. B. H., & House, L. L. (2019). A deep learning based approach to forecast the onset of magnetic substorms. *Space Weather*, *17*, 1534–1552. https://doi.org/10.1029/2019SW002251

Marshall, R. A., Dalzell, M., Waters, C. L., Goldthorpe, P., & Smith, E. A. (2012). Geomagnetically induced currents in the New Zealand power network. *Space Weather*, *10*(8), S08003. https://doi.org/10.1029/2012SW000806

Mayaud, P. N. (1973). *A hundred year series of geomagnetic data, 1868–1967: Indices aa, storm sudden commencements (SSC)* (p. 256). IUGG Publ. Office.

McKinney, W. (2010). *Data structures for statistical computing in Python*. Retrieved from http://conference.scipy.org/proceedings/scipy2010/mckinney.html

McPherron, R. L., Aubry, M. P., Russell, C. T., & Coleman, P. J. (1973). *Satellite studies of magnetospheric substorms on august 15, 1968 4. Ogo 5 magnetic field observations*. (Vol. 78, Tech. Rep. No. 16). Retrieved from https://www.researchgate.net/profile/Robert_Mcpherron/publication/254933902_Satellite_Studies_of_Magnetospheric_Substorms_on_August_15_1968/links/5adf4d5aa6fdcc29358e13ed/Satellite-Studies-of-Magnetospheric-Substorms-on-August-15-1968.pdf

Morley, S., & Freeman, M. P. (2007). On the association between northward turnings of the interplanetary magnetic field and substorm onsets. *Geophysical Research Letters*, *34*(8). https://doi.org/10.1029/2006GL028891

Morley, S., Rouillard, A., & Freeman, M. (2009). Recurrent substorm activity during the passage of a corotating interaction region. *Journal of Atmospheric and Solar-Terrestrial Physics*, *71*(10–11), 1073–1081. https://doi.org/10.1016/J.JASTP.2008.11.009

Ngwira, C. M., Pulkkinen, A., Bernabeu, E., Eichner, J., Viljanen, A., & Crowley, G. (2015). Characteristics of extreme geoelectric fields and their possible causes: Localized peak enhancements. *Geophysical Research Letters*, *42*(17), 6916–6921. https://doi.org/10.1002/2015GL065061

Ngwira, C. M., Pulkkinen, A., Leila Mays, M., Kuznetsova, M. M., Galvin, A. B., Simunac, K., et al. (2013). Simulation of the 23 July 2012 extreme space weather event: What if this extremely rare CME was Earth directed? *Space Weather*, *11*(12), 671–679. https://doi.org/10.1002/2013SW000990

Ngwira, C. M., Pulkkinen, A., Wilder, F. D., & Crowley, G. (2013). Extended study of extreme geoelectric field event scenarios for geomagnetically induced current applications. *Space Weather*, *11*(3), 121–131. https://doi.org/10.1002/swe.20021

Odstrcil, D. (2003). Modeling 3-D solar wind structure. *Advances in Space Research*, *32*(4), 497–506. https://doi.org/10.1016/S0273-1177(03)00332-6

Oliveira, D., Arel, D., Raeder, J., Zesta, E., Ngwira, C. M., Carter, B. A., et al. (2018). Geomagnetically induced currents caused by interplanetary shocks with different impact angles and speeds. *Space Weather*, *16*(6), 636–647. https://doi.org/10.1029/2018SW001880

Oliveira, D., & Samsonov, A. (2018). Geoeffectiveness of interplanetary shocks controlled by impact angles: A review. *Advances in Space Research*, *61*(1), 1–44. https://doi.org/10.1016/J.ASR.2017.10.006

Oughton, E. J., Hapgood, M., Richardson, G. S., Beggan, C. D., Thomson, A. W. P., Gibbs, M., et al. (2019). A risk assessment framework for the socioeconomic impacts of electricity transmission infrastructure failure due to space weather: An application to the United Kingdom. *Risk Analysis*, *39*(5), 1022–1043. https://doi.org/10.1111/risa.13229

Oughton, E. J., Skelton, A., Horne, R. B., Thomson, A. W. P., & Gaunt, C. T. (2017). Quantifying the daily economic impact of extreme space weather due to failure in electricity transmission infrastructure. *Space Weather*, *15*(1), 65–83. https://doi.org/10.1002/2016SW001491

Owens, M., Lang, M., Barnard, L., Riley, P., Ben-Nun, M., Scott, C. J., et al. (2020). A computationally efficient, time-dependent model of the solar wind for use as a surrogate to three-dimensional numerical magnetohydrodynamic simulations. *Solar Physics*, *295*(3), 43. https://doi.org/10.1007/s11207-020-01605-3

Owens, M., & Riley, P. (2017). Probabilistic solar wind forecasting using large ensembles of near-sun conditions with a simple one-dimensional Upwind Scheme. *Space Weather*, *15*(11), 1461–1474. https://doi.org/10.1002/2017SW001679

Oyedokun, D., Heyns, M., Cilliers, P., & Gaunt, C. (2020). Frequency components of geomagnetically induced currents for power system modelling. In *2020 International Saupec/Robmech/Prasa Conference* (pp. 1–6). IEEE. https://doi.org/10.1109/SAUPEC/RobMech/PRASA48453.2020.9041021

Pedregosa, F., Varoquaux, G., Gramfort, A., Michel, V., Thirion, B., Grisel, O., et al. (2011). Scikit-learn: Machine learning in Python. *Journal of Machine Learning Research*, *12*, 2825–2830. http://jmlr.org/papers/v12/pedregosa11a.html

Pulkkinen, A., Lindahl, S., Viljanen, A., & Pirjola, R. (2005). Geomagnetic storm of 29–31 October 2003: Geomagnetically induced currents and their relation to problems in the Swedish high-voltage power transmission system. *Space Weather*, *3*(8), S08C03. https://doi.org/10.1029/2004SW000123

Richardson, I. G., & Cane, H. V. (2012). Near-earth solar wind flows and related geomagnetic activity during more than four solar cycles (1963–2011). *Journal of Space Weather and Space Climate*, *2*, A02. https://doi.org/10.1051/swsc/2012003

Rodger, C. J., Mac Manus, D. H., Dalzell, M., Thomson, A. W. P., Clarke, E., Petersen, T., et al. (2017). Long-term geomagnetically induced current observations from New Zealand: Peak current estimates for extreme geomagnetic storms. *Space Weather*, *15*(11), 1447–1460. https://doi.org/10.1002/2017SW001691

Rogers, N. C., Wild, J. A., Eastoe, E. F., Gjerloev, J. W., & Thomson, A. W. P. (2020). A global climatological model of extreme geomagnetic field fluctuations. *Journal of Space Weather and Space Climate*, *10*, 5. https://doi.org/10.1051/swsc/2020008

Shore, R. M., Freeman, M. P., Coxon, J. C., Thomas, E. G., Gjerloev, J. W., & Olsen, N. (2019). Spatial variation in the responses of the surface external and induced magnetic field to the solar wind. *Journal of Geophysical Research: Space Physics*, *124*(7), 6195–6211. https://doi.org/10.1029/2019JA026543

Smith, A. W., Freeman, M. P., Rae, I. J., & Forsyth, C. (2019). The influence of sudden commencements on the rate of change of the surface horizontal magnetic field in the United Kingdom. *Space Weather*, *17*, 1605–1617. https://doi.org/10.1029/2019SW002281

Smith, A. W., Rae, I. J., Forsyth, C., Oliveira, D. M., Freeman, M. P., & Jackson, D. R. (2020). Probabilistic forecasts of storm sudden commencements from interplanetary shocks using machine learning. *Space Weather*, *18*(11), e2020SW002603. https://doi.org/10.1029/2020SW002603

Takeuchi, T., Araki, T., Viljanen, A., & Watermann, J. (2002). Geomagnetic negative sudden impulses: Interplanetary causes and polarization distribution. *Journal of Geophysical Research*, *107*(A7), 1096. https://doi.org/10.1029/2001JA900152

Tanskanen, E., Pulkkinen, T. I., Koskinen, H. E. J., & Slavin, J. A. (2002). Substorm energy budget during low and high solar activity: 1997 and 1999 compared. *Journal of Geophysical Research*, *107*(A6), 1086. https://doi.org/10.1029/2001JA900153

Thomson, A. W., Dawson, E. B., & Reay, S. J. (2011). Quantifying extreme behavior in geomagnetic activity. *Space Weather*, *9*(10). https://doi.org/10.1029/2011SW000696

Thomson, A. W., McKay, A. J., Clarke, E., & Reay, S. J. (2005). Surface electric fields and geomagnetically induced currents in the Scottish Power grid during the 30 October 2003 geomagnetic storm. *Space Weather*, *3*(11), S11002. https://doi.org/10.1029/2005sw000156

Turnbull, K. L., Wild, J. A., Honary, F., Thomson, A. W. P., & McKay, A. J. (2009). Characteristics of variations in the ground magnetic field during substorms at mid latitudes. *Annales Geophysicae*, *27*(9), 3421–3428. https://doi.org/10.5194/angeo-27-3421-2009

Turner, D. L., O'Brien, T. P., Fennell, J. F., Claudepierre, S. G., Blake, J. B., Kilpua, E. K. J., & Hietala, H. (2015). The effects of geomagnetic storms on electrons in Earth's radiation belts. *Geophysical Research Letters*, *42*(21), 9176–9184. https://doi.org/10.1002/2015GL064747

Van Der Walt, S., Colbert, S. C., & Varoquaux, G. (2011). The NumPy array: A structure for efficient numerical computation. *Computing in Science & Engineering*, *13*(2), 22–30. https://doi.org/10.1109/MCSE.2011.3

Viljanen, A., Amm, O., & Pirjola, R. (1999). Modeling geomagnetically induced currents during different ionospheric situations. *Journal of Geophysical Research: Space Physics*, *104*(A12), 28059–28071. https://doi.org/10.1029/1999JA900337

Viljanen, A., Nevanlinna, H., Pajunpää, K., & Pulkkinen, A. (2001). Time derivative of the horizontal geomagnetic field as an activity indicator. *Annales Geophysicae*, *19*(9), 1107–1118. https://doi.org/10.5194/angeo-19-1107-2001

Viljanen, A., & Pirjola, R. (1994). Geomagnetically induced currents in the Finnish high-voltage power system. *Surveys in Geophysics*, *15*(4), 383–408. https://doi.org/10.1007/BF00665999

Viljanen, A., Pirjola, R., Prácser, E., Ahmadzai, S., & Singh, V. (2013). Geomagnetically induced currents in Europe: Characteristics based on a local power grid model. *Space Weather*, *11*(10), 575–584. https://doi.org/10.1002/swe.20098

Viljanen, A., Tanskanen, E. I., & Pulkkinen, A. (2006). Relation between substorm characteristics and rapid temporal variations of the ground magnetic field. *Annales Geophysicae*, *24*(2), 725–733. https://doi.org/10.5194/angeo-24-725-2006

Virtanen, P., Gommers, R., Oliphant, T. E., Haberland, M., Reddy, T., Cournapeau, D., et al. (2020). SciPy 1.0: Fundamental algorithms for scientific computing in Python. *Nature Methods*, *17*, 261–272. https://doi.org/10.1038/s41592-019-0686-2

Wang, C., Li, C. X., Huang, Z. H., & Richardson, J. D. (2006). Effect of interplanetary shock strengths and orientations on storm sudden commencement rise times. *Geophysical Research Letters*, *33*(14), L14104. https://doi.org/10.1029/2006GL025966

Yue, C., Zong, Q. G., Zhang, H., Wang, Y. F., Yuan, C. J., Pu, Z. Y., et al. (2010). Geomagnetic activity triggered by interplanetary shocks. *Journal of Geophysical Research*, *115*(A5), A00I05. https://doi.org/10.1029/2010JA015356

Zhang, J. J., Wang, C., Sun, T. R., Liu, C. M., & Wang, K. R. (2015). GIC due to storm sudden commencement in low-latitude high-voltage power network in China: Observation and simulation. *Space Weather*, *13*(10), 643–655. https://doi.org/10.1002/2015SW001263

Zhou, X., & Tsurutani, B. T. (2001). Interplanetary shock triggering of nightside geomagnetic activity: Substorms, pseudobreakups, and quiescent events. *Journal of Geophysical Research*, *106*(A9), 18957–18967. https://doi.org/10.1029/2000JA003028